Fabrication and characterization of micro-structures created by direct laser writing in multi-layered chalcogenide glasses

Casey M. Schwarz[a], Chris N. Grabill[a], Benn Gleason[b,c], Gerald D. Richardson[a], Anna M. Lewis[a], Aadit Vyas[a], Clara Rivero-Baleine[b,e], Kathleen A. Richardson[b], Alexej Pogrebnyakov[d], Theresa S. Mayer[d], Stephen M. Kuebler[a,b,f*]

[a]Chemistry Department, University of Central Florida, Orlando, FL 32816, USA
[b]CREOL, The College of Optics and Photonics, University of Central Florida, Orlando, FL 32816, USA
[c]Materials Science and Engineering Department, Clemson University, Clemson, SC 29634, USA
[d]Department of Electrical Engineering, Pennsylvania State University, University Park, PA 16802, USA
[e]Lockheed Martin, Orlando, FL 32819, USA
[f]Physics Department, University of Central Florida, Orlando, FL 32816, USA

*kuebler@ucf.edu; Tele: +1 407-823-3720; Fax: +1 407-823-2252; http://npm.creol.ucf.edu

ABSTRACT

Arsenic trisulfide (As_2S_3) is a chalcogenide (ChG) material with excellent infrared (IR) transparency (620 nm to 11 μm), low phonon energies, and large nonlinear refractive indices. These properties directly relate to commercial and industrial applications including sensors, photonic waveguides, and acousto-optics. Multi-photon exposure can be used to photo-pattern thermally deposited As_2S_3 ChG glassy films of molecular clusters. Immersing the photo-patterned cross-linked material into a polar-solvent removes the unexposed material leaving behind a structure that is a negative-tone replica of the photo-pattern. Nano-structure arrays that were photo-patterned in single-layered As_2S_3 films through multi-photon direct laser writing (DLW) resulted in the production of nano-beads as a consequence of a standing wave effect. To overcome this effect, an anti-reflective (AR) layer of arsenic triselenide (As_2Se_3) was thermally deposited between the silicon substrate and the As_2S_3 layer, creating a multi-layered film. The chemical composition of the unexposed and photo-exposed multi-layered film was examined through Raman spectroscopy. Nano-structure arrays were photo-patterned in the multi-layered film and the resulting structure, morphology, and chemical composition were characterized, compared to results from the single-layered film, and correlated with the conditions of the thermal deposition, patterned irradiation, and etch processing.

Keywords: Arsenic trisulfide, arsenic triselenide, chalcogenide glass, multi-photon, direct laser writing, microstructures, standing wave.

1. INTRODUCTION

Infrared (IR) optics have many applications including detectors, sensors and imaging systems. The production of light-weight, low-profile, robust optics with good thermal properties is necessary to achieve many of these applications. Conventional IR optics are likely to contain costly single-crystal Ge, Si, or ZnSe materials which make them bulky, heavy, and expensive. In addition to this, conventional processing techniques, such as diamond turning, also adds cost to the production while less expensive alternatives such as precision glass molding, produces heavy optics with limited functionality.[1, 2] These factors limit high volume commercial production of optical systems.

Advanced Fabrication Technologies for Micro/Nano Optics and Photonics VIII, edited by Georg von Freymann, Winston V. Schoenfeld, Raymond C. Rumpf, Proc. of SPIE Vol. 9374, 937403 · © 2015 SPIE
CCC code: 0277-786X/15/$18 · doi: 10.1117/12.2077629

Chalcogenide glasses (ChGs) are multi-component materials that can be manufactured and processed more quickly with less expense than single-component crystalline IR optics. ChGs can also have lower coefficients of thermal expansion (CTE) and lower changes in refractive index with temperature (dn/dt) making them tunable and functional over a range of conditions and environments.

As_2S_3 ChGs are amorphous semiconductors with high transparency in the IR region (620 nm to 11 μm), with an optical bandgap Eg = 2.35 eV ($\lambda \sim 517$ nm) and a refractive index of n = 2.45 - 2.53.[3-5] As_2S_3 ChGs are known to be photosensitive and can change both their optical and chemical properties under photoexposure. As_2S_3 films can be thermally deposited and photo-patterned, like polymeric photo-resists, then chemically etched to obtain a targeted structure.[4, 6] Three-dimensional (3D) structures including photonic crystals, nanowires, and waveguides have been fabricated in As_2S_3 films via multi-photon direct laser writing (DLW).[4, 7-9] As_2S_3 ChG film physical and chemical structure and properties are known to be sensitive to the thermal deposition method.[6] The morphology of the fabricated structure is directly related to the local irradiance distribution of the focused beam.

In this work, the structure, morphology, and appearance of nano-structures created by DLW in As_2S_3 films is related to the etch conditions, thermal deposition parameters, chemical composition, and the addition of an anti-reflection (AR) coating of As_2Se_3 to the substrate. Reflection of the focused laser beam at the silicon substrate back into the interaction volume of the material is shown to produce standing wave interference which modulates the film exposure with distance from the substrate. In order to minimize this interference, an AR coating of As_2Se_3 was added between the substrate and the material.[10] By exploring the addition of an AR coating and creating a multi-layered ChG film, processing conditions have been identified that enable precise control over structure size and shape for targeted applications. The chemical composition for unexposed, UV exposed, and laser exposed films are related to the etch response, nano-structure formation, and deposition conditions of the individual films.

2. METHODOLOGY

2.1. Thermal deposition of thin films

Two types of photo-sensitive films were studied in this work: a single-layered As_2S_3 film and a multi-layered film consisting of As_2S_3 on an AR-layer of As_2Se_3, as illustrated in Fig. 1. For the single-layered film, As_2S_3 was deposited onto polished silicon wafers by thermal evaporation of the bulk glass. The temperature of the substrate was not controlled. The film was deposited at a rate of 27 Å s^{-1}, had a thickness of 1075 nm ± 0.8 nm, and appeared pink in color. For the multi-layered film, a layer of As_2Se_3 was deposited first on polished silicon wafers followed by thermal evaporation of a layer of As_2S_3. The As_2Se_3 layer was deposited at a rate of 4 Å s^{-1}, had a thickness of 203 nm ± 3 nm. The As_2S_3 layer was deposited at a rate of 30 Å s^{-1} and had a thickness of 896 nm ± 13 nm. The multi-layer film appeared silver to light green. The temperature of the substrate was not controlled. All films were transported in petri dishes wrapped with aluminum foil and stored in an amber desiccator to prevent unintended exposure to ambient light. It is important to note that a different thermal deposition tool was used to deposit the single-layered film than was used to deposit the multi-layered film.

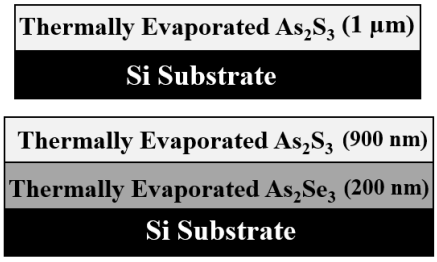

Figure 1. Diagrams of the single-layered and multi-layered film.

2.2. Direct laser writing and UV exposure

DLW was conducted using a continuous-wave mode-locked femtosecond laser (Coherent-Mira, 800-nm center wavelength, 120-fs pulse duration, 76 MHz repetition rate). An acousto-optic modulator (AOM) was used for the electronic control of the intensity of the laser beam. The laser beam was directed through beam expanders to a 100×/1.4 *NA* oil-immersion objective (Nikon) which focused the beam into the film/substrate interface. A coordinate system is defined such that the substrate lies in the *xy*-plane and the beam is focused along the *z*-axis. The average power used to cross-link the films was measured at the exit aperture of the objective lens using an integrating sphere and found to range from 0.05 mW to 0.50 mW. To define the pattern, the sample was translated at a speed of 50 μm s^{-1} in the *x*-, *y*-, and *z*-axes relative to the laser beam. Single-point, nano-scale feature arrays were photo-patterned by locating the beam to a targeted (*x*,*y*)-position, exposing the region at a certain power controlled by the AOM, then translating the sample in the *z*-direction over a distance of 4 μm. This ensured that features were exposed throughout the entire thickness of the film. UV-exposed films were prepared by irradiating film samples for two minutes in a Zeta Loctite UV flood chamber equipped with high-pressure mercury lamps that emit broad-band UV radiation (65 mW/cm^2).

2.3. Etch development

The etch rate of the unexposed single-layered and multi-layered films was measured by immersing the films in solutions of 0.5 mol-% diisopentylamine (DIPA) dissolved in dimethylsulfoxide (DMSO) and monitoring visually with a camera to identify the time required to remove the unexposed material. Eq. 1 defines the etch rate for a given film as the ratio of its thickness to the time required to etch it.

$$\text{Etch Rate} = \frac{\text{Film Thickness}}{\text{Etch Duration}} \tag{1}$$

The same etching method and 0.5 mol-% solution was used for the development of photo-patterned nano-structures. The developed nano-structures also underwent additional rinsing steps following chemical etching. The nano-structures were rinsed for 15 seconds in a fresh solution of DIPA in DMSO then immersed in IPA for 2 minutes. A scanning electron microscope (SEM, Zeiss ULTRA-55 FEG) was used to record top-down and profile images of the As_2S_3 nano-structures. These images were used to determine the dimensions and shapes of the features so these could be correlated with film composition, processing conditions, and fabrication laser power.

2.4. Characterization

The chemical composition of unexposed, UV exposed, and laser exposed films was explored using micro-Raman spectroscopy. Two instruments were used for this study. A Horiba Jobin Yvon LabRamHR high resolution confocal Raman microscope system with an average power of 80 mW at the output and an excitation wavelength of 785 nm was used. The laser power was adjusted using neutral density filters to reduce undesired photo-modifications of the films during the measurements. The beam was focused with a 100× microscope objective (*NA* = 0.9, *WD* = 0.21 mm) giving a spatial resolution of 2 microns. A Bruker Senterra micro Raman system with an average power of 10 mW and an excitation wavelength of 785 nm was also used. The incoming laser beam was focused onto the front polished surface of the sample using a 10× microscope objective (*NA* = 0.30, *WD* = 15 mm) without attenuation. The resulting focused beam diameter was 50 – 200 μm. The refractive index of unexposed, UV exposed, and laser exposed films was determined using a variable-angle ellipsometer (Woollam M2000, 0.24 μm - 1.7 μm). Focusing optics were used to characterize sample areas as small as 100 × 100 μm^2 with a spectral resolution of 3 nm at visible wavelengths and 6 nm in the near infrared.

3. RESULTS AND ANALYSIS

3.1. Etch characteristics

In our previous work with single-layered As_2S_3 thin films it was found that 0.5 mol-% DIPA in DMSO is below the saturation limit of the solution and completely etches films up to 1 μm in thickness in under 2 minutes.[6] Visual

observations revealed that a 30 minute etch time was required to completely remove the As_2S_3 layer from the multi-layered films (Table 1). The As_2Se_3 layer was intact up to an hour after immersion in 0.5 mol-% DIPA in DMSO. The deposition conditions (base pressure, deposition pressure, deposition rate, film thickness) were all kept relatively constant from single-layer to multi-layer deposition and the only significant change was the addition of the As_2Se_3 layer.

Table 1. Color of single- and multi-layered films as a function of etching time.

Film	Etching time / min			
	0	1	5	30
Single-layered	Pink	Silver	--	--
Multi-layered	Silver/Green	Green	Blue	Light Pink

The Raman spectra measured from the single-layered and multi-layered films are shown in Fig. 2. Peaks were assigned as described in References 5 and 11.[1, 5, 11] The silicon substrate produces the peak at 300 cm^{-1}. The presence of As_2S_3 glass is confirmed by adsorptions at 232 cm^{-1} and 136 cm^{-1}, As_4S_4 subunits are confirmed by absorption at 222 cm^{-1}, As_4S_4 and As-As homopolar bonds are confirmed by absorptions at 363 cm^{-1} and 191 cm^{-1}, and AsS_3 subunits are confirmed by absorption at 346 cm^{-1}. Features indicative of the As_2Se_3 layer include As_2Se_3 adsorptions at 223 cm^{-1}, As_4Se_3 at 237 cm^{-1}, and Se_8 rings at 252 cm^{-1}.

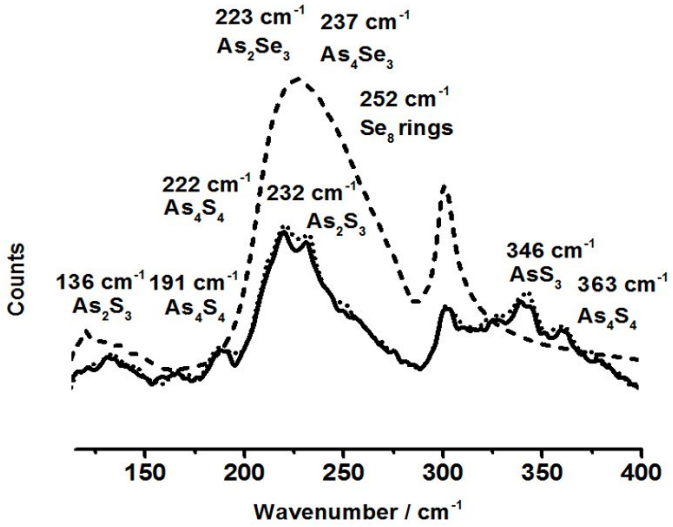

Figure 2. Raman spectra of the multi-layered pristine film (dotted line), the multi-layered film after 5 minute etch (solid line), and the multi-layered film after 30 minute etch (dashed line) with peaks identified.

Visual observation and Raman spectra both indicate that five minutes of etching time was sufficient to remove all As_2S_3 from the single-layered film. In contrast, an etching period as long as 30 minutes was needed to remove the sulfide layer from the multi-layered film. Raman spectra were measured for the multi-layered films after several intervals of etching, rinsing, and drying (Fig. 2). The Raman spectra show little difference after 5 minutes of etching. After 30 minutes of etching, peaks indicative of the As_2S_3 layer are absent and those corresponding to the AR As_2Se_3 layer are larger. These experiments indicate that 30 minutes was needed to completely remove the As_2S_3 layer from the multi-layer films.

Although the sulfide layers of the single- and multi-layered films were deposited under identical conditions, the difference in etch time suggests that the presence of the As_2Se_3 AR layer alters the structure of the sulfide layer. Structural differences were not apparent from Raman spectra of the pristine single- and multi-layer films (Fig. 3). Compositionally, both single-layered and multi-layered films share similar peaks; however, the peak ratios between features located from 325 cm^{-1} to 125 cm^{-1} are significantly different. This peak enlargement may be due to contribution from the Raman excitation of the As_2Se_3 layer beneath the As_2S_3 layer during measurements. The difference in etch time

may result from slight compositional differences due to different thermal deposition chamber and calibration, and thermal dissipation due to stage temperature control and the presence of an AR layer.

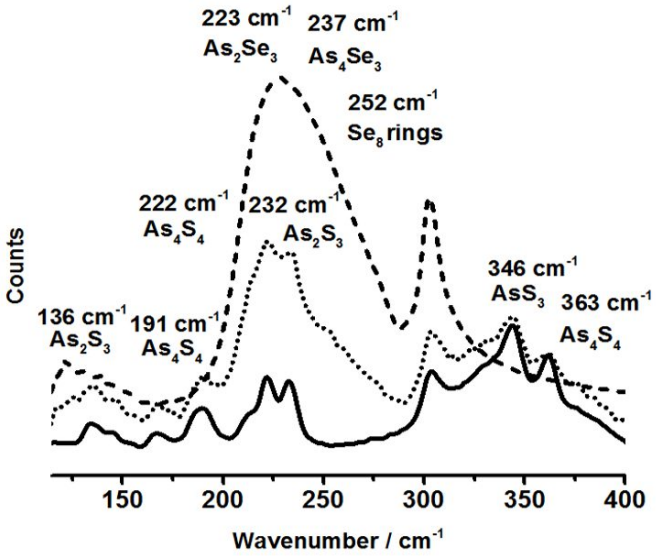

Figure 3. Raman spectra of the single-layered film (solid line), multi-layered film (dotted line) and the As_2Se_3 layer (dashed line).

3.2. Fabricated nano-structure arrays

Although the DLW patterning was intended to produce cylindrical pillars, exposure in the single-layered film generated stacks of nanobeads. This occurs because the focused beam reflects at the higher index silicon substrate back into the material producing a standing wave interference that modulates the film exposure with distance from the substrate. To reduce this effect, the multi-layer films were produced, with the sandwiched As_2Se_3 film functioning as an AR coating that mitigates back-reflection of the focused laser beam. AR coatings can be made with layers having a physical thickness of $m\lambda_0/4n$, where λ_0 is the vacuum wavelength of the laser beam, n is the refractive index of the material, and m = 1, 3, 5…. For the multi-layer films studied here, the 200-nm thickness of As_2Se_3 acts as a ¾λ AR coating at λ_0 = 800 nm.

A set of sixteen arrays, each a 9 × 9 grid of single-point exposures with a 500 nm pitch were photo-patterned in the single-layer and the multi-layered film over a range of average (avg) focused laser powers (0.02 mW - 0.50 mW) then etched in 0.5 mol-% DIPA in DMSO. Dose arrays patterned in the multi-layered film were compared to patterned nano-structures in the single-layered film (Fig. 4). Nano-structures patterned in the multi-layered film were nearly cylindrical in shape, as intended. The absence of the standing-wave effect avoids intensity modulation and resulting "pinch-off" of the structure near the interface that is observed with the single-layer films. As a result, the multi-layer film enabled narrower features to be patterned with better overall surface adhesion. The increase in substrate adhesion is due to increased surface area between the substrate and the nano-structure which led to smaller features surviving the etch processing without delaminating or collapsing. With these improvements in structure formation and adhesion, the rest of this paper will focus on nano-structures fabricated in multi-layered film.

Structures were not observed for powers lower than 0.16 mW in the multi-layered film. This is due to the laser power being too low to induce sufficient cross-linking, and the resulting nano-structures were either not robust enough to survive etching or would delaminate during the solution processing. Structure delamination is already evident at 0.16 mW, as seen in Fig. 5A. Above this power, the width of the features steadily increased, and adjacent features began to overlap at powers larger than 0.26 mW. Below this power, features appear to be well defined and sufficiently resolved; however, some proximity effects nearest the center are visible. The proximity effect may be due to the integrated exposure resulting when adjacent features are exposed, unresolved etching, and a cumulative thermal effect.

No film ablation was observed indicating that powers below 0.50 mW are sufficient to cause cross-linking in the material without damage to the silicon substrate. As seen in Fig. 5B, the feature dimensions follow a characteristic power relationship curve and features as small as ~120 nm were observed.

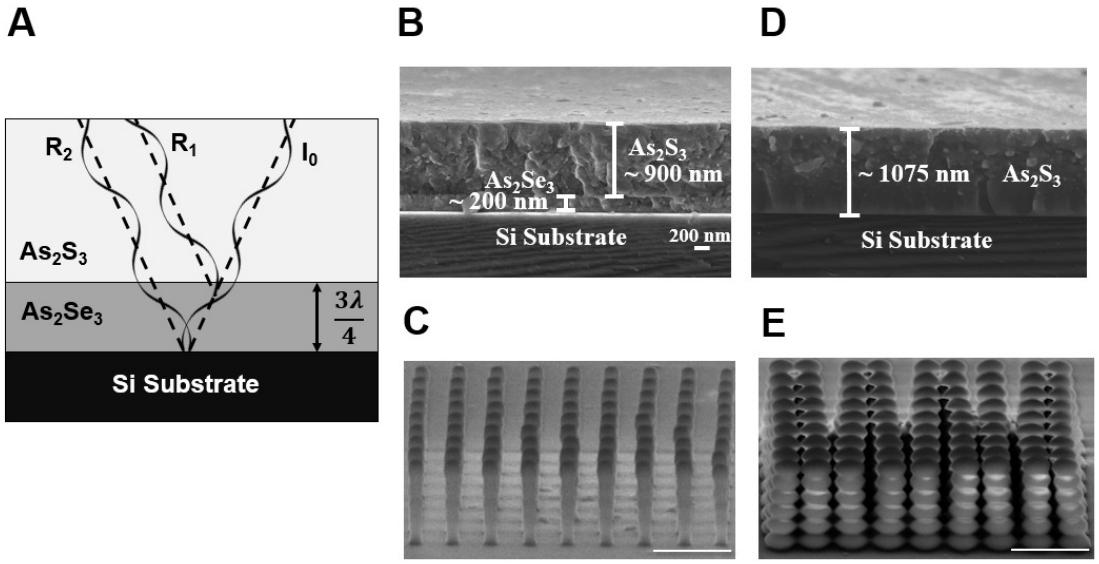

Figure 4. (**A**) Schematic of interference resulting from an interface bearing a three-quarter-wave AR coating (I_0 is the incident beam and R_1 and R_2 are the reflected beams). (**B**) Cleaved profile of As_2S_3 on As_2Se_3 and (**C**) fabricated nano-structures. (**D**) Cleaved profile of As_2S_3 and (**E**) fabricated nano-structures (scale bar corresponds to 1 μm).

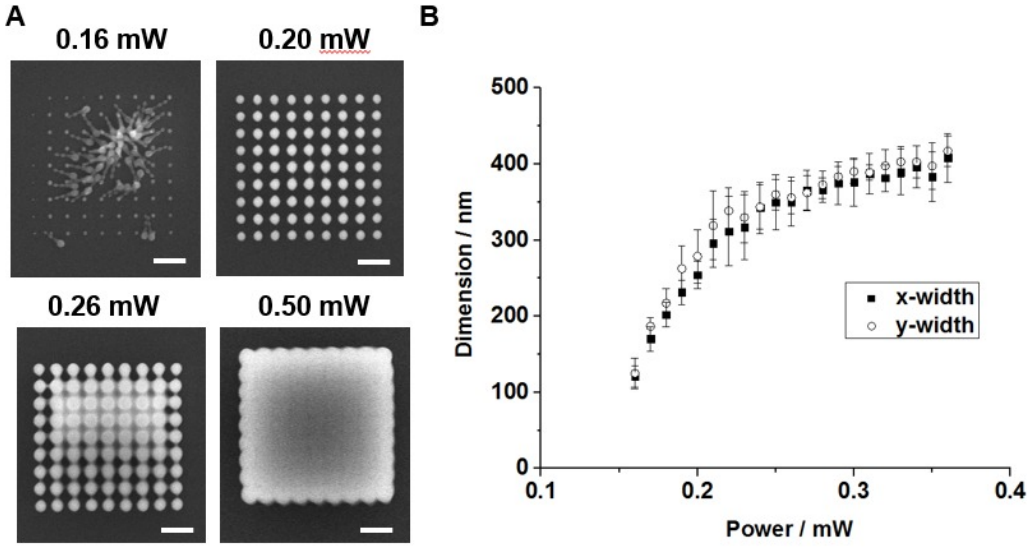

Figure 5. (**A**) SEM images of selected nano-structured photo-patterned As_2S_3 on As_2Se_3 film using powers ranging from 0.16 mW to 0.50 mW. (**B**) X-width (filled in squares) and y-width (open circles) measurements for nano-structures fabricated in As_2S_3 on As_2Se_3 film (scale bar corresponds to 1 μm).

Due to the increased control over feature shape and substrate adhesion, large arrays of homogenous nano-structures could be fabricated. A nano-structure array of 250 μm × 250 μm was successfully fabricated in the multi-layer

As_2S_3-on-As_2Se_3 film. The pillars were observed to be of consistent and homogenous widths and heights (Fig. 6). These large pillar arrays demonstrate reproducibility and scalability and the ability to change the fill-factor and thus refractive index and optical functionality of large areas.

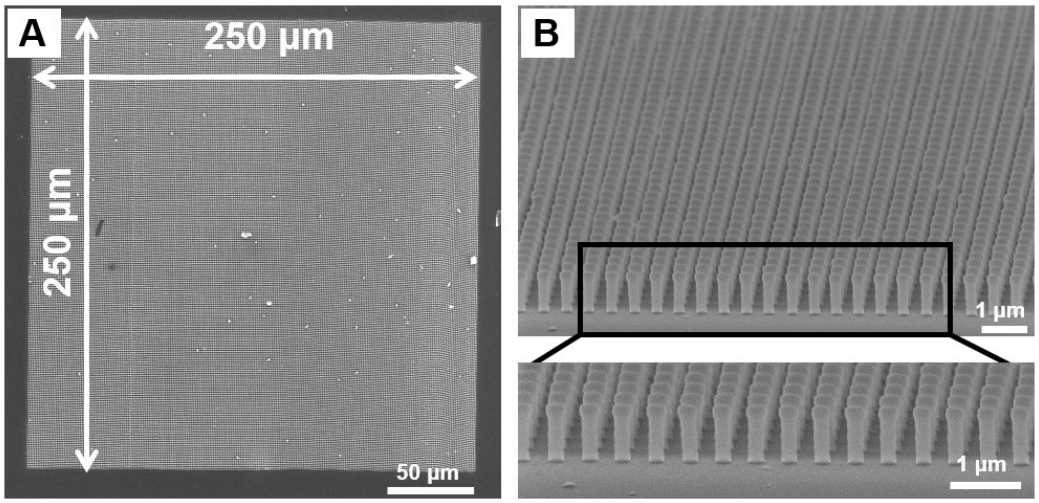

Figure 6. SEM images of (**A**) 250 µm ×250 µm nano-structured pillar array with (**B**) profile images.

3.3. Micro-Raman characterization of unexposed and exposed films

Micro-Raman spectroscopy was used to identify the presence of molecular fragments in unexposed, UV-exposed, and laser exposed multi-layered films. Thermal deposition fragments the bulk As_2S_3 glassy network solid into molecular clusters (As_4S_6, As_4S_4, and S_8).[5, 11] These molecular clusters are then thermally deposited onto the substrate forming a metastable glassy photosensitive film. This film can then be photo-crosslinked back to the As_2S_3 network via photoexcitation.[4] Molecular clusters of As_4S_6, As_4S_4, S_8, and other clusters containing homopolar As-As and S-S bonds are responsible for a film's photosensitivity.

Raman spectra from unexposed, UV-exposed, and laser-exposed multi-layered films are presented in Fig. 7. The peaks are assigned as described in Sect. 3.1 and References 5 and 11. UV-exposure decreases the amplitude of a peak associated with As_4S_4 homopolar bonds (191 cm^{-1}) and increases the amplitude of a peak assigned to heteropolar AsS_3 units (346 cm^{-1}). These changes are consistent with photo-induced cross-linking of the material, as we reported previously for single-layered films.[6] However, other homopolar bonds (222 cm^{-1}) are seen to increase after UV exposure. This is mostly like due to the influence of the As_2Se_3 AR coating layer and not evidence of (or lack of) cross-linking.

When the multi-layer film was exposed to the focused laser beam, the ratio of homopolar to heteropolar bonds changed to a greater extent than was seen with UV exposure. In this case, the homopolar bonds of interest (191 cm^{-1}, 222 cm^{-1}) were seen to decrease. Laser irradiation caused the As_4S_4 molecular clusters to reorganize or cross-link and begin to form the original glass network indicated by the decrease in the homopolar bonds. Zoubir and co-workers also studied Raman measurements from laser-exposed thermally deposited As_2S_3 films.[5] These films were single-layered 1.6 µm thick As_2S_3, but the peaks can still be used to compare to our laser-exposed multi-layered film. Measured Raman spectra of the laser-exposed multi-layered film show a similar decrease in low frequency peaks (191 cm^{-1}, 222 cm^{-1}, 232 cm^{-1}) assigned to As_4S_4 and As_2S_3. The S-S peak was also seen to decrease near the 494 cm^{-1} peak. There was a slight difference in observed spectral detail and distinction observed in the low frequency peaks. This may come from the difference in Raman excitation wavelength (785 nm vs. 840 nm) and influence of the underlying As_2Se_3 layer. The excitation wavelength and proximity of electronic transitions within the material can alter the intensity of the Raman signal and peak detail.

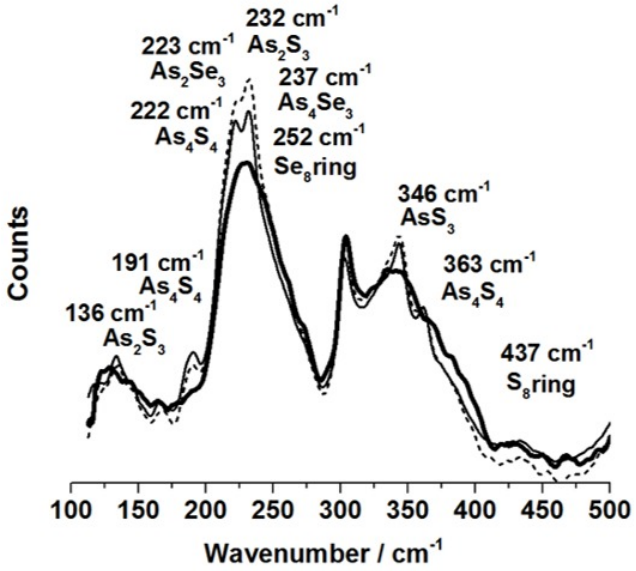

Figure 7. Raman spectra of the unexposed (thin line), UV-exposed (dashed line) and laser-exposed (thick line) for the multi-layered film with peaks identified.

4. CONCLUSIONS

Thermally deposited multi-layered As_2S_3 on As_2Se_3 films were found to be photo-patternable by multi-photon DLW, consistent with the behavior of single-layered As_2S_3 films. The structure, morphology, and appearance of fabricated nano-structures was related to the etch response, deposition conditions, and chemical composition of the thermally deposited multi-layered films. Raman spectroscopy measurements of the multi-layered film showed molecular cluster peaks known to be responsible for photosensitivity. Evidence of increased cross-linking with laser-exposure over that of UV exposure was seen. By incorporating an AR coating consisting of an etch-resistant As_2Se_3 layer between the ChG fabrication layer and the Si substrate, the standing wave interference was significantly reduced. This resulted in the generation of nano-structures with cylindrical shapes, better substrate adhesion, with smaller dimensions (widths of ~ 120 nm) and more predictable fill fractions when compared to stacked bead shaped nano-structures fabricated in single-layered films. Control over the standing wave effect and better resulting substrate adhesion lead to the ability to fabricate areas of homogenous nano-structures over large areas (250 μm × 250 μm) which has important implications for manufacturing and commercial applications.

5. ACKNOWLEDGMENTS

This work was partially supported by NSF CAREER award DMR/CHE-0748712; Lockheed Martin; the Florida High Tech Corridor Council; the Space Research Initiative Program, through the Florida Space Institute hosted at the University of Central Florida; and the National Aeronautics and Space Administration through the University of Central Florida's NASA-Florida Space Grant Consortium. Anna Lewis was supported by a UCF SURF Scholarship. We thank Dr. Pieter Kik and Mr. Chatdanai Lumdee for assistance with the ellipsometry measurements.

6. REFERENCES

[1] Zhang, X.H., Guimond, Y., and Bellec, Y., "Production of complex chalcogenide glass optics by molding for thermal imaging," J. Non-Cryst. Solids, 326, 519-524 (2003).

[2] Cha, D.H., Kim, H.-J., Hwang, Y., *et al.*, "Fabrication of molded chalcogenide-glass lens for thermal imaging applications," Appl. Opt., 51(23), 5649-5656 (2012).

[3] Hilton, A.R., Sr., [Chalcogenide glasses for infrared optics], McGraw-Hill Companies, Inc., New York City, 1-304 (2010).
[4] Wong, S., Deubel, M., Perez-Willard, F., *et al.*, "Direct laser writing of three-dimensional photonic crystals with a complete photonic bandgap in chalcogenide glasses," Adv. Mater., 18(3), 265-269 (2006).
[5] Zoubir, A., Richardson, M., Rivero, C., *et al.*, "Direct femtosecond laser writing of waveguides in As_2S_3 thin films," Opt. Lett., 29(7), 748-750 (2004).
[6] Schwarz, C.M., Williams, H.E., Grabill, C.N., *et al.* "Processing and properties of arsenic trisulfide chalcogenide glasses for direct laser writing of 3D micro structures," Proc. SPIE 8974, 89740P-1 - 89740P-11, (2014).
[7] Nicoletti, E., Bulla, D., Luther-Davies, B., *et al.*, "Wide-angle stop-gap chalcogenide photonic crystals generated by direct multiple-line laser writing," Appl. Phys. B, 105(4), 847-850 (2011).
[8] Nicoletti, E., Bulla, D., Luther-Davies, B., *et al.*, "Generation of λ/12 nanowires in chalcogenide glasses," Nano. Lett., 11(10), 4218-4221 (2011).
[9] Nicoletti, E., Zhou, G., Jia, B., *et al.*, "Observation of multiple higher-order stopgaps from three-dimensional chalcogenide glass photonic crystals," Opt. Lett., 33(20), 2311-2313 (2008).
[10] Hasan, S.F. and Turki, S.N., "Design of an antireflection coating for mid- wave infrared regions in the range (3000-5000) nm," International Journal of Application or Innovation in Engineering & Management, 2(11), 96-100 (2013).
[11] Iovu, M.S., Kamitsos, E.I., Varsamis, C.P.E., *et al.*, "Raman spectra of As_xSe_{100-x} and $As_{40}Se_{60}$ glasses doped with metals," Chalcogenide Lett., 2(3), 21-25 (2005).